ACS APPLIED MATERIALS & INTERFACES

Research Article

www.acsami.org

Synergetic Role of Li^+ during Mg Electrodeposition/Dissolution in Borohydride Diglyme Electrolyte Solution: Voltammetric Stripping Behaviors on a Pt Microelectrode Indicative of Mg–Li Alloying and Facilitated Dissolution

Jinho Chang,[†] Richard T. Haasch,[‡] Jinwoo Kim,[§] Timothy Spila,[‡] Paul V. Braun,[§] Andrew A. Gewirth,*[,†] and Ralph G. Nuzzo*[,†]

[†]Department of Chemistry, University of Illinois, Urbana, Illinois 61801, United States

[‡]Frederick Seitz Materials Research Laboratory, University of Illinois, Urbana, Illinois 61801, United States

[§]Department of Materials Science and Engineering, Frederick Seitz Materials Research Laboratory, University of Illinois at Urbana–Champaign, Urbana, Illinois 61801, United States

Supporting Information

ABSTRACT: We describe a voltammetric and spectroscopic study of Mg electrodeposition/dissolution ($Mg_{Dep/Dis}$) in borohydride diglyme electrolyte solution containing Li^+ carried out on a Pt ultramicroelectrode (UME, r = 5 μm). The data reveal Li^+ cation facilitation that has not been previously recognized in studies made using macroelectrodes. While a single broad, asymmetric stripping peak is expected following Mg_{Dep} on a Pt macroelectrode in 0.1 M $Mg(BH_4)_2$ + 1.5 M $LiBH_4$ diglyme solution on a Pt UME, the stripping reveals three resolved oxidation peaks, suggesting that $Mg_{Dep/Dis}$ consists of not only a Mg/Mg^{2+} redox reaction but also contributions from Mg–Li alloying/dissolution reaction processes. Detailed XPS, SIMS, ICP, and XRD studies were performed that confirm the importance of Mg–Li alloy formation processes, the nature of which is dependent on the reduction potential used during the Mg_{Dep} step. Based on the electrochemical and surface analysis data, we propose an electrochemical mechanism for $Mg_{Dep/Dis}$ in a borohydride diglyme electrolyte solution that, in the presence of 1.5 M Li^+ ions, proceeds as follows: (1) $Mg^{2+} + 2e^- \rightleftharpoons Mg$; (2) $(1-x)Mg^{2+} + xLi^+ + (2-x)e^- \rightleftharpoons Mg_{(1-x)}Li_x$, $0 < x \leq 0.02$; and (3) $(1-y)Mg^{2+} + yLi^+ + (2-y)e^- \rightleftharpoons Mg_{(1-y)}Li_y$, $0.02 < y \leq 0.09$. Most significantly, we find that the potential-dependent $Mg_{Dep/Dis}$ kinetics are enhanced as the concentration of the $LiBH_4$ in the diglyme electrolyte is increased, a result reflecting the facilitating influences of reduced uncompensated resistance and the enhanced electro-reduction kinetics of Mg^{2+} due to Mg–Li alloy formation.

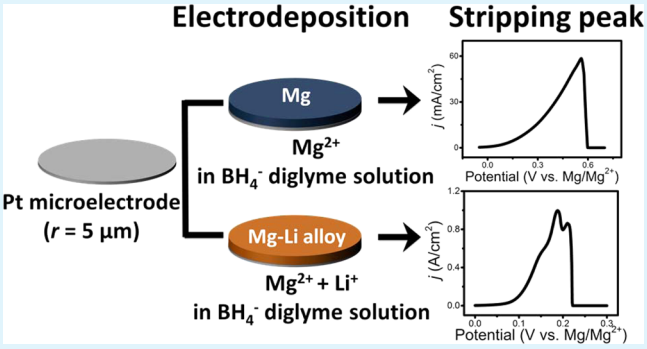

KEYWORDS: *Pt microelectrode, Mg rechargeable battery, Mg electrodeposition/dissolution, stripping peak, Mg–Li alloy, magnesium borohydride*

1. INTRODUCTION

The Mg electrodeposition/dissolution reaction ($Mg_{Dep/Dis}$) is considered to be a promising anode reaction for use in a rechargeable, high-volumetric-density Mg battery. The reversibility of the $Mg_{Dep/Dis}$ processes, however, is dependent on electrolyte composition, and most organic solvents and conventional salts fail to demonstrate reversible behavior during $Mg_{Dep/Dis}$ due to the formation of passivation films.[1] Aurbach et al.[2] reported that ether electrolyte solutions with $AlCl_{(3-n)}R_n + R_2Mg$ exhibit near 100% Coulombic efficiency for $Mg_{Dep/Dis}$. Corrosive behaviors in working electrode systems were reported to result, however, due to the presence of the chloride anion in an Mg-organohaluminate electrolyte.[3,4] As an alternative electrolyte, Mohtadi et al.[5] reported a reversible, halide-free $Mg_{Dep/Dis}$ system containing $Mg(BH_4)_2$ dissolved in a THF or DME solution. Additionally, this group reported that addition of $LiBH_4$ as an additive in DME enhanced both the current densities and the Coulombic efficiency of $Mg_{Dep/Dis}$. Following that report, Shao et al.[6] observed an interesting phenomenon that the addition of $LiBH_4$ dramatically enhances the $Mg_{Dep/Dis}$ kinetics in the diglyme borohydride electrolyte. Detailed electrochemical mechanisms of $Mg_{Dep/Dis}$ occurring both with and without $LiBH_4$ in the diglyme solution have not been reported, however, and thus, the synergistic effects of the Li^+ on the electrochemistry in this electrolyte remain incompletely understood.

Received: October 24, 2014
Accepted: January 6, 2015
Published: January 6, 2015

DOI: 10.1021/am507375t
ACS Appl. Mater. Interfaces 2015, 7, 2494–2502

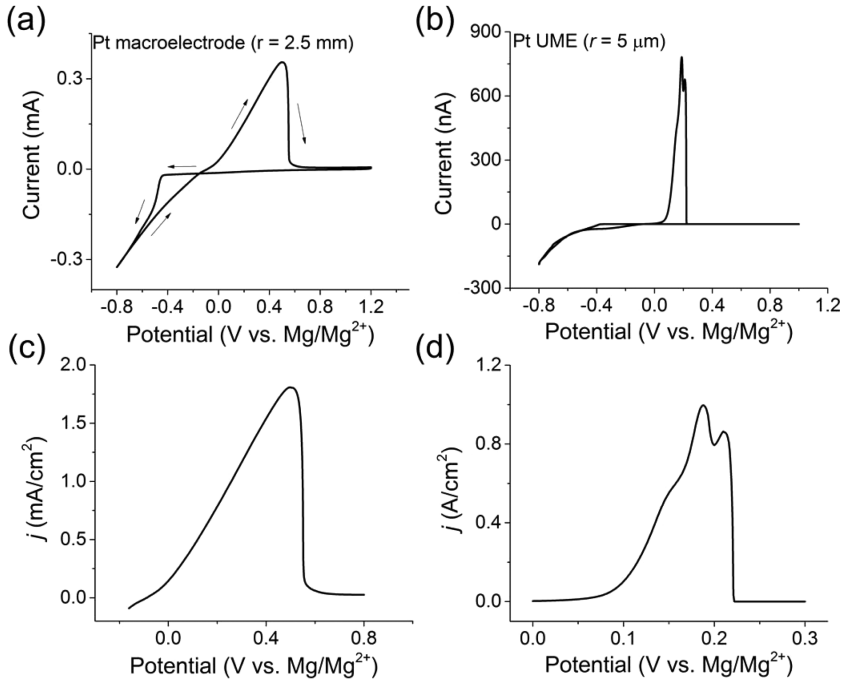

Figure 1. Twentieth cycle CVs of $Mg_{Dep/Dis}$ in 0.1 M $Mg(BH_4)_2$ + 1.5 M $LiBH_4$ diglyme solution on (a) a Pt macroelectrode (r = 2.5 mm), (b) a Pt UME (r = 5 μm), and (c and d) their corresponding stripping peaks.

The development of a high-performance metal-anode chemistry for use in Mg rechargeable batteries is a matter of great current interest in research, and significant efforts have been made to develop and better understand the electrochemistry of the Mg/Mg^{2+} electrochemical system. From a technical perspective, a high concentration of Mg^{2+} (>0.01 M) is desirable to achieve high theoretical energy densities. The study of Mg anodes under such conditions, however, is difficult due to severe voltammetric distortions that result from the large iR drop that occurs in solutions made with low dielectric constant solvents. In such cases, the use of an ultramicroelectode (UME) is particularly advantageous for electroanalysis because the iR drop can be reduced to negligible levels due to the small magnitude of the currents passed in the UME.[7] Numerous examples of electrochemical measurements made using the UMEs in challenging contexts are available in the literature.[8−12]

Mg−Li alloys have been the subject of extensive studies motivated by the potential uses of this low-density material in the automobile, electronic, and aerospace industries. Zhang et al.[13−16] reported direct electrodeposition of Mg−Li alloys on inert electrodes from high-temperature chloride melts. The electrochemical Mg−Li alloying/dealloying reaction has also been the subject of study, and Sohn et al.[17,18] reported lithiation of a Mg/C composite electrode. The phase transition suggested for the electrochemical Mg−Li alloy formation is reported as (1) Mg → α-Mg (Mg-rich phase) and (2) α-Mg → β-Li (Li- rich phase). Thermodynamically speaking, the reduction potential for each phase should be different, and thus, distinct voltammetric peaks should possibly be monitored for a sequence of phase evolution.[19] Such behaviors during the electrochemical formation of Mg−Li alloys have not been reported, however.[17]

In this report, we describe the results of electrochemical and correlated physicochemical characterization studies made using a Pt UME to probe $Mg_{Dep/Dis}$ processes occurring in a borohydride diglyme electrolyte solution containing Li^+. The current data demonstrate complex electrochemical dynamics, including the resolution of three oxidation peaks, which are associated with the formation and dissolution of Mg and Mg−Li alloys of different compositions. The data from electrochemical, physical, and spectroscopic analyses demonstrate that Li^+ ions foster a synergistic enhancement of the electrochemistry of Mg in ethereal borohydride electrolyte solutions.

2. EXPERIMENTAL SECTION

2.1. Chemicals. Magnesium borohydride ($Mg(BH_4)_2$, 95%), lithium borohydride ($LiBH_4$, ≥ 95%), diethylene glycol dimethyl ether (diglyme, anhydrous, 99.5%), and tetrahydrofuran (THF, anhydrous, ≥ 99.9%) were purchased from Sigma-Aldrich and used without further purification.

2.2. Electrochemical Measurements. A Pt ultramicroelectrode (UME) with radius, r = 5 μm was purchased from CH Instruments, Inc. (Austin, TX). A Pt macroelectrode was prepared by DC sputtering (AJA International, Inc., Scituate, MA) using an Ar plasma. A silicon wafer with a ca. 300 nm thick oxide (University Wafer, Boston, MA) was first coated with a 6.0 nm adhesion layer of Ti, followed by ca. 300 nm Pt at 50 W and 3 mTorr Ar. Deposition rates of Ti and Pt were ca. 0.3 and 1.0 Å/s, respectively. For the Mg macroelectrode, a 0.1 mm thick Mg foil was used. MicroCut Disks (1200G/P2500) were used for polishing the foil (Buehler, Lake Bluff, IL). To minimize oxide layer formation, we performed the polishing process in an Ar filled glovebox. Electrochemical measurements were performed in a three-electrode cell configuration using Pt or Mg as the working electrode and polished Mg ribbons as both the counter and reference electrodes, respectively. Li bulk deposition and Li underpotential deposition (upd) measurements were performed using a Pt electrode with Li ribbon for the reference and counter electrodes. Potentials are reported versus Mg/Mg^{2+}. For macroelectrode measurements, a home-built, enclosed, Teflon electrochemical cell was used. Microelectrode measurements were performed using an enclosed 5 mL glass vial. A CH 660D potentiostat (CH Instruments, Inc., Austin, TX) was used for all electrochemical measurements. For cyclic voltammetry, the scan rate in all experiments was 0.02 V/s. All

DOI: 10.1021/am507375t
ACS Appl. Mater. Interfaces 2015, 7, 2494−2502

electrochemical experiments were performed inside an Ar filled glovebox, where [H_2O] and [O_2] were <0.1 and <5 ppm, respectively.

2.3. Materials Characterization. X-ray photoelectron spectroscopy measurements were performed using a Kratos AXIS Ultra spectrometer with a monochromatic Al Kα (1486.6 eV) X-ray source. High-resolution spectra were collected with 40 eV pass energy, and the binding energy scale was referenced to the aliphatic C 1s peak at 285 eV.

Secondary ion mass spectrometry (SIMS) measurements were made using a Cameca IMS 5F spectrometer. A 200 nA O_2^+ primary ion beam was accelerated to 12 kV voltage and rastered on the sample over a 200 × 200 μm area. The secondary ions were collected in the magnetic sector mass analyzer using a 750 μm field aperture and 150 μm contrast diaphragm. Secondary ions were collected on an electron multiplier for count rates between 1 to 10^5 counts per second (cps) and on a Faraday cup for higher count rates. Jumps in the data from ~10^5 to 10^6 cps are due to switching between the detectors. The sputtering rate was determined by measuring the crater depth using a Dektak 3ST stylus profilometer. X-ray diffraction (XRD) measurements were carried out using a PANalytical X'pert MRD system at angle of incidence $\Omega = 1°$, with a detector (2θ) scan step size of 0.02°, at 0.5 s per step. The $\Omega = 1°$ angle of incidence was chosen to facilitate characterization of the electrodeposited film. Inductively coupled plasma (ICP) analyses were performed by using a ELAN DRC-e ICP-MS operated in the School of Chemical Sciences Microanalysis Laboratory. The morphology of the Mg–Li deposit was characterized using a field-emission scanning electron microscope (FESEM, Hitachi S-4700).

3. RESULTS AND DISCUSSION

3.1. Electrochemistry of Mg/Mg^{2+} Occurring on Pt Macro- and Microelectrodes. The electrochemical behaviors of Mg during deposition and dissolution shows marked sensitivity to its voltammetric cycling history; Mg becomes more stable in nature after an activation phase of several deposition and dissolution cycles, which is mainly associated with the elimination of impurities adsorbed on the Pt surface during the $Mg_{Dep/Dis}$ cycling. Representative data for the latter are shown in Figure 1a, which shows data from the 20th cyclic voltammogram (CV) obtained from a Pt macroelectrode immersed in a solution containing 0.1 M $Mg(BH_4)_2$ + 1.5 M $LiBH_4$ dissolved in diglyme. On the cathodic sweep the CV is flat until a potential of ca. −0.43 V vs Mg/Mg^{2+}, where the CV shows the onset of reductive behavior. Reversing the scan direction leads to a decrease in reduction current and then one broad, asymmetric oxidation peak after 0 V is reached. This behavior is in agreement with CV data reported previously in the literature.[6] Figure 1b shows the corresponding 20th cycle voltammetry data obtained using a Pt UME immersed in the same solution. The onset of a reductive current on the cathodic scan also occurs at −0.4 V, with a continuous increase in its magnitude as the potential becomes more negative. Electrodeposition onto a UME typically exhibits limiting behavior,[12] and the limiting current i_{ss} given by eq 1

$$i_{ss} = 4nFCDr \quad (1)$$

where F is Faraday's constant, C is the bulk concentration of Mg^{2+}, r is the UME radius, n is the number of electrons transferred (n = 2), and D is the diffusion coefficient. The magnitude of D was estimated by using a potentiostatic transient method on the UME (Figure S1, Supporting Information) and found to be ca. 1 × 10^{-6} cm^2/s. Using this value, we estimated that the steady state current should be ca. 30 nA. However, Figure 1b shows that the reductive current at the UME is substantially greater than this value and approaches 190 nA. Because this current is higher than the limiting current expected from the UME, it must be the case that the reductive process occurring on the UME is not limited to Mg electrodeposition alone, but must also include contributions from other processes.

Figure 1b also shows that the stripping peak from the UME is substantially more complex, leaving resolved features relative to generally broad peaks shapes obtained with the macroelectrode. Figure 1c,d compares the stripping peaks from the two electrodes more directly. While the stripping peak from the macroelectrode is essentially featureless (Figure 1c), that from the UME (Figure 1d) is resolved into three distinct peaks, seen here at 0.15, 0.19, and 0.21 V, respectively. The presence of at least three distinct stripping features highly suggests that the dissolution process can be attributed to three distinct oxidation reactions.

The presence of three oxidation peaks on a Pt UME is directly related to the presence of Li^+ in the borohydride diglyme solution. In CVs measured without the addition of $LiBH_4$, only one stripping peak is observed, which must be associated with Mg dissolution. These data also evidence substantially lower current densities relative to that for electrolyte solutions containing Li^+ (Figure S2, Supporting Information). The effect of $LiBH_4$ concentration on the overall kinetics of $Mg_{Dep/Dis}$ is discussed in detail in sections that follow.

The quantitative attributes of the three oxidation peaks observed in the Pt UME voltammetry data in the presence of $LiBH_4$ are markedly dependent on the limiting cathodic polarization potential, E_{Red}. The data in Figure 2a shows representative CVs obtained on cycling from 1 V to different values of E_{Red}. As E_{Red} becomes more negative, the magnitude of the integrated deposition current increases. Figure 2b shows that, at E_{Red} = −0.5 V, only one stripping peak at 0.15 V is observed (Peak A). When E_{Red} is increased to −0.62 V, a second stripping peak is evident centered at ~0.19 V (Peak B). A third oxidation peak, seen at 0.23 V (Peak C) finally emerges at values of E_{Red} = −0.7 V. The emergence of the three discrete stripping peaks strongly suggests that they originate from three mechanistically distinct electro-reduction processes.

Figure 2c shows a quantitative analysis of the stripping charges, $Q_{stripping}$, obtained by integrating mathematical fits made to deconvolute the oxidation peaks (A, B, and C) seen as a function of E_{Red}. To do so, the primary data were fit assuming that the three oxidation reactions were ideally Nernstian, and the number of transferred electrons = 2, assumptions validated by analyses discussed in detail below. On the basis of these assumptions, we set the total width at half-height for each of the stripping peaks, $\Delta E_{p,1/2}$, equal to 45.3 mV, and each peak fit with a Gaussian line shape.[20] The main points established by this analysis are that the integrated magnitudes of the charge associated with peak A, $Q_{stripping,A}$, continuously increases as E_{Red} became more negative, reaching a value of 2.3 C/cm^2 at a limiting E_{Red} = −0.8 V. The onset of nonzero values of $Q_{stripping,B}$ was evidenced when limiting values of E_{Red} reached ~ −0.6 V, a value some 0.1 V more negative than that seen for the onset of $Q_{stripping,A}$. The processes mediating the deposition of the B-state material are quite efficient, and $Q_{stripping,B}$ values reached 3.1 C/cm^2 at E_{Red} = −0.8 V. The apparent onset of $Q_{stripping,C}$ contributions occurred at more cathodic potentials, at values of E_{Red} near −0.7 V with $Q_{stripping,C}$ reaching 2.9 C/cm^2 at E_{Red} = −0.8 V. By way of comparison, an equivalent integrated stripping current for a monolayer of Mg on polycrystalline Pt

DOI: 10.1021/am507375t
ACS Appl. Mater. Interfaces 2015, 7, 2494–2502

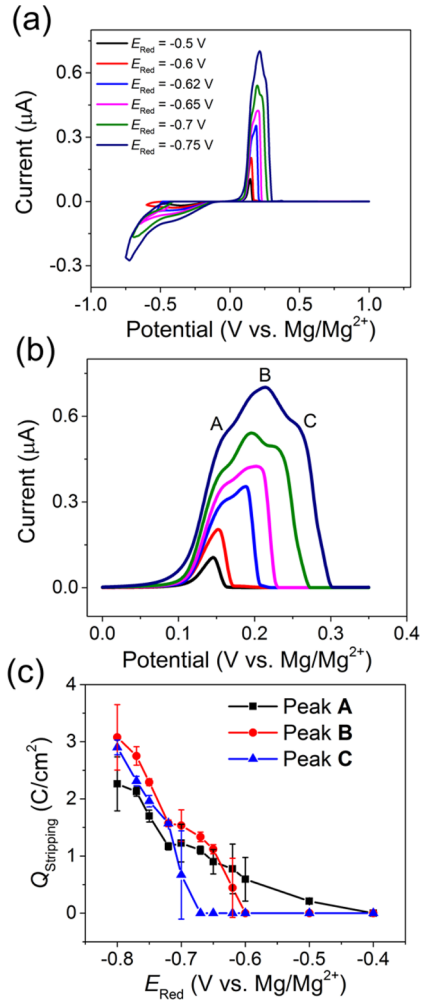

Figure 2. (a) CVs on a Pt UME (r = 5 μm) cycled from 1 V to different E_{Red} in 0.1 M $Mg(BH_4)_2$ + 1.5 M $LiBH_4$ diglyme solution, (b) their stripping peaks at different E_{Red}, and (c) estimated stripping charges from each oxidation peak, A, B, and C as a function of E_{Red}.

would yield a charge of ca. 420 $\mu C/cm^2$, assuming a close-packed arrangement of Mg (atomic radius = 145 pm) with a two electron transfer occurring with 100% Coulombic efficiency, a number which is a factor of 7×10^3 smaller than the total stripping charge found here. The data thus reveal that the oxidation peaks represent the stripping of essentially bulk-like material from the Pt electrode surface.

We next address the impacts of $LiBH_4$ alone on the voltammetry of the Pt UME. Figure 3 shows CVs obtained from a solution containing 1.5 M $LiBH_4$ in diglyme. The CV presented in Figure 3a shows that the onset of the lithiation of Pt occurs at −0.88 V versus Mg/Mg^{2+}. This potential is substantially more negative than that utilized in the Mg deposition measurements described above. The data demonstrate that bulk lithiation alone cannot be responsible for the complex stripping behaviors observed when Mg^{2+} is present in the electrolyte. A deeper insight into the electrodynamics of the Pt/Li^+ system is affected by an analysis of the CV data presented in Figure 3b, which shows the presence of a reduction peak at −0.47 V versus Mg/Mg^{2+} and a corresponding oxidation peak at −0.35 V versus Mg/Mg^{2+}. Integration of these peaks shows that the charge associated with adsorption/stripping in this case is ~256 $\mu C/cm^2$, a value close to that expected for a monolayer of Li (210 $\mu C/cm^2$) on a polycrystalline Pt surface, assuming a close-packing arrangement of Li with one electron transfer. On the basis of this close correspondence of charges, we associate these new peaks with Li upd on the Pt surface. We note that prior work showed Li upd on Pt in THF occurs at approximately the same potentials.[21,22] This observation strongly suggests that Li is present as a upd adlayer on Pt at the potentials at which bulk Mg deposition occurs. The presence of Li on the electrode surface during the Mg deposition process suggests that Li and Mg may form an alloy. Indeed, prior studies have suggested that upd adlayers can facilitate nucleation and growth in alloy formation processes.[16,23−25]

To test whether a mechanism involving alloy formation might be the origin of the complex UME voltammetry observed in the $Li/Mg\ BH_4^-$ system, we carried out a systematic study using an electrolyte solution containing 1.5 M $NaBH_4$ + 0.1 M $Mg(BH_4)_2$ while keeping other conditions the same as those used in the prior Li^+-based experiments. This provides an essential control of bulk growth behaviors because Mg does not form a stable alloy with Na at room temperature.[26] The CV data presented in Figure S3 (Supporting Information) show that in this case only a Mg^{2+} reduction process occurs on the Pt UME in diglyme solution. The CV exhibits only a single stripping peak in contrast to the more complex behavior found with Li. Together, the data support the conclusion that the three peak stripping behavior seen above is one associated with electro-reduction mechanism involving Li−Mg alloy formation.

3.2. XPS, SIMS, and XRD Characterization of Mg−Li Alloy Formation. To better characterize the mechanism

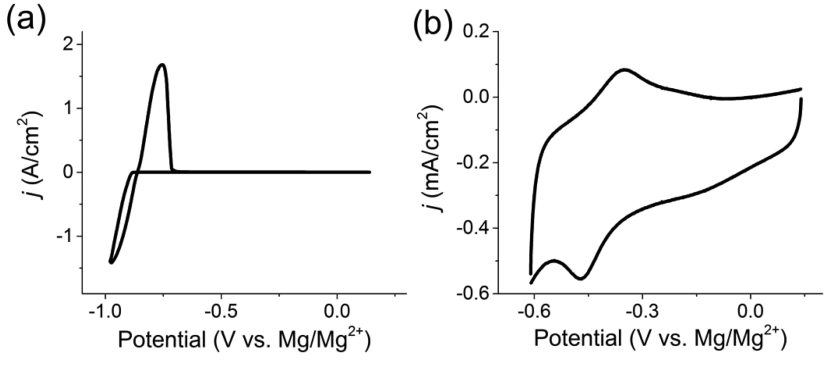

Figure 3. CVs (a) for the bulk lithiation and (b) for the Li upd/desorption on a polycrystalline Pt UME (r = 5 μm) obtained in 1.5 M $LiBH_4$ diglyme solution.

DOI: 10.1021/am507375t
ACS Appl. Mater. Interfaces 2015, 7, 2494−2502

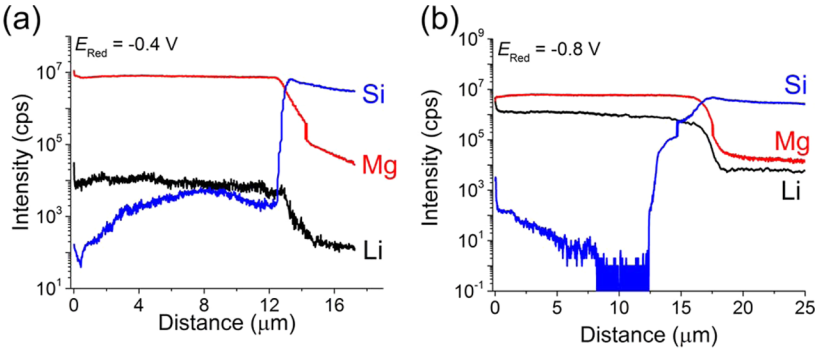

Figure 4. SIMS depth profiles from deposited films at (a) E_{Red} = −0.4 V and (b) −0.8 V. Electrodeposition was performed for 5 h at given E_{Red} in 0.1 M $Mg(BH_4)_2$ + 1.5 M $LiBH_4$ diglyme solution.

positing the formation of a Li−Mg alloy, we obtained SIMS data from films electrodeposited at different values of E_{Red}. The results are presented in Figure 4, which shows SIMS depth profiles measured from films electrodeposited from solutions polarized for 5 h at E_{Red} = −0.4 and −0.8 V (Figures 4a and b, respectively). In the film prepared at E_{Red} = −0.4 V, a signal for Li was detected at relatively low intensity until the signal associated with Si increased, indicating the end of the metallic electrode. The interfacial mixing indicated by the Mg and Si ion intensities likely results from the ion-milling process, an inference supported by control experiments. We note that the Pt signal is not shown in these data as conditions that optimizing the instrument for analyses of Mg and Li were used. The Pt signal is found in control experiments, as is illustrated by the SIMS data shown in Figure S4 (Supporting Information).

The SIMS data obtained from films deposited at E_{Red} = −0.8 V, also shown in Figure 4b, exhibit substantially increased Li intensities relative to the data for deposition carried out at E_{Red} = −0.4 V. The intensity of the Li signal is now several orders of magnitude higher and evidenced throughout the full extent of the Mg deposit. These data compel the finding that a codeposition of Li and Mg occurs and that the amount of Li in the Mg−Li deposit is strongly dependent on E_{Red}.

Figure 5a shows high-resolution XPS spectra obtained in the energy region associated with the Li 1s and Mg 2p core levels for films prepared at different values of E_{Red}. We should note that a small amount of Mg (68.4 nmol/cm^2) was deposited even by applying E_{Red} = −0.2 V for 5 h as shown in the corresponding *i*−*t* curve in Figure S5 (Supporting Information). With E_{Red} = −0.2 V, the XPS shows a peak associated with Mg^{2+} (likely MgO at 50.1 eV) and a smaller one associated with Mg(0) (48.4 eV).[27] MgO is formed on the surface as a result of the air exposure that occurs during transfer from the glovebox to the XPS vacuum chamber. For films prepared at E_{Red} = −0.4 V, a peak at 59.2 eV is evidenced, which is associated with a bulk plasmon excitation from Mg metal.[28] A weak peak at 55.4 eV is assigned to the Li 1s peak from Li_2O, again a product formed as a result of oxidation occurring during sample transfer.[28,29] At E_{Red} = −0.8 V, the Li 1s core-level peak is more intense, indicating the presence of substantial Li in the film at this deposition potential, a finding in agreement with the SIMS profiles described above. The upper graph in Figure 5b shows the Mg 2p peaks associated with Mg^{2+} and Mg(0) present in the films electrodeposited at E_{Red} = −0.6 V (black) and E_{Red} = −0.8 V (red), respectively. For these plots, a baseline was subtracted from high energy resolution data, and

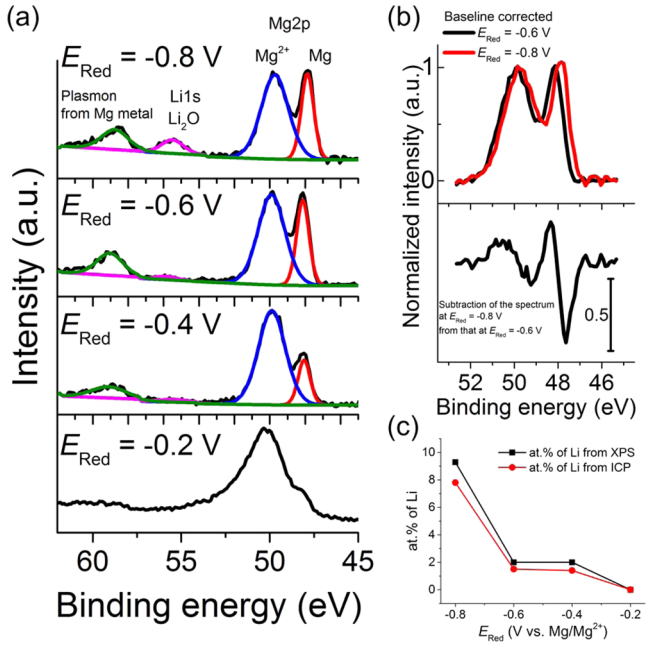

Figure 5. (a) High-resolution XPS spectra from films prepared at different E_{Red}. (b, upper) Mg 2p peaks associated with Mg^{2+} and Mg(0) in XPS spectrum obtained from the films electrodeposited at E_{Red} = (black) −0.6 V and (red) −0.8 V, respectively and (lower) spectra generated by subtracting the signal of Mg 2p peaks obtained from electrodeposited film at E_{Red} = −0.8 V from that at E_{Red} = −0.6 V. (c) Atomic percent of Li from Mg−Li deposits prepared at different E_{Red}; at.% of Li over Mg in each film was estimated by both XPS (black ■) and ICP analysis (red ●), respectively. All Mg−Li deposits were electrodeposited at different E_{Red} in 0.1 M $Mg(BH_4)_2$ + 1.5 M $LiBH_4$ diglyme solution for 5 h.

the intensities of the two spectra normalized to the magnitude of the Mg^{2+} peak. The subtracted XPS spectra (Figure 5b lower) shows that the binding energy of the Mg 2p peak associated with Mg^{2+} in the two spectra are, in fact, similar (as expected for it being a native oxide formed post-deposition). The peak associated with Mg(0), however, shifts to lower binding energy as E_{Red} is progressively polarized from −0.6 to −0.8 V. The subtracted XPS spectra clearly show that the binding energy of Mg 2p peak associated with Mg(0) from the film at E_{Red} = −0.8 V was 0.65 eV lower than that from the film electrodeposited at E_{Red} = −0.6 V; this shift clearly indicates Mg−Li alloy formation.[30,31]

The data in Figure 5c reports on the atomic percent (at.%) of Li in the Li−Mg film obtained as a function of E_{Red} as assessed

DOI: 10.1021/am507375t
ACS Appl. Mater. Interfaces 2015, 7, 2494−2502

via surface limited (ca. 3 nm) XPS analyses and ICP microanalysis of the full deposit. The figure shows that Li is present in the Mg film even at E_{Red} =-0.4 V, and the amount of Li increases as E_{Red} becomes more negative. There is a dramatic increase in the amount of Li incorporated into the film between E_{Red} = −0.6 V and −0.8 V. The data in Figure 5c suggest that there are effectively three different mechanistic regions, each corresponding to different values of E_{Red}. In the first region (E_{Red} = −0.4 V), relatively little Li is incorporated in the Mg deposit. In the second region (−0.8 < E_{Red} < −0.4 V), intermediate Li concentrations are found. At E_{Red} = −0.8 V, the Li concentration in the deposit becomes quite substantial, approaching 10 at.%. Taken together with the SIMS data, the phase present in the latter case must result from dynamics that lead to full bulk incorporation of Li in the Mg deposit. The atomic structure of this phase is discussed in detail in the sections that follow. Also, we observed that the at.% of Li over Mg at the surface measured by XPS was slightly higher than that in the bulk as measured by ICP in the deposits prepared at E_{Red} = −0.4, −0.6, and −0.8 V. The observed greater at.% of Li over Mg at the surface than in the bulk of the Mg−Li alloy deposits could possibly be associated with an SEI layer containing Li^+. However, the observed ∼100% Coulombic efficiency in $Mg_{Dep/Dis}$ estimated by CVs obtained in a diglyme electrolyte solution containing 0.1 M $Mg(BH_4)_2$ and 1.5 M $LiBH_4$ indicates the absence of or negligible amount of SEI layer containing Li^+, which is well-known to block Mg^{2+} ion transport.

We carried out X-ray diffraction studies to characterize the atomic structure of the Mg deposits/alloys afforded by this electrolyte system. Figure 6a shows an XRD pattern obtained

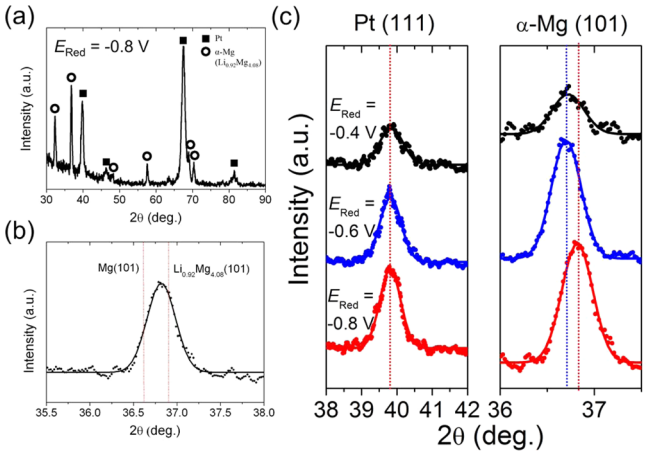

Figure 6. (a) Wide-range XRD pattern of a deposited film at E_{Red} = −0.8 V on a Pt macroelectrode, (b) a peak from α-Mg (101) plane, and (c) peaks from a Pt (111) and a α-Mg (101) plane on deposited films at different E_{Red}, (black) −0.4, (blue) −0.6, and (red) −0.8 V. All Mg−Li films were electrodeposited for 5 h.

from a film deposited chronoamperometrically at E_{Red} = −0.8 V for 5 h on a Pt macroelectrode. The peaks indicated in Figure 6a are assignable to either the underlying Pt substrate or an electrodeposited Mg−Li alloy. The literature provides no explicit match for the diffraction data presented here. The best fit found corresponds to the reflections and spacings of $Li_{0.92}Mg_{4.08}$ (PDF 03-065-4080), although significant strains in relation to that phase are in evidence. The lattice parameters (a and c) estimated from peaks attributed to (100) and (101) planes at 2θ = 32.36 and 36.90°, respectively, are listed in Table 1. The film deposited at E_{Red} = −0.8 V exhibits both a and c

Table 1. Lattice Parameters Estimated from α-Mg (100) and (101) Peaks

structure	lattice parameter	
	a (Å)	c (Å)
Mg	3.21	5.21
$Li_{0.92}Mg_{4.08}$	3.19	5.13
this work (E_{Red} = −0.8 V)	3.19	5.18

parameters that are shortened compared to those for bulk Mg, while a was close to that in $Li_{0.92}Mg_{4.08}$. We note that differences between our film and $Li_{0.92}Mg_{4.08}$ are to be expected because our film contains only one-half the amount of Li relative to the literature standard (ca. 9% Li vs 18.4%). To better illustrate these features, the peak from the (101) plane of the Mg−Li alloys deposited at E_{Red} = −0.4, −0.6, and −0.8 V are compared in Figure 6c. The data in the figure show that this peak shifts to higher values as E_{Red} is shifted cathodically, indicating a Mg−Li alloy formation with more Li in the structure as E_{Red} becomes more negative. To verify the observed shift was not an artifact, we compared a Pt (111) peak in each XRD pattern as a standard, and this peak position did not change as a function of E_{Red}.

To further confirm that the Mg−Li deposit was not a mixture of Li and Mg metals but rather their alloy, we investigated Li diffusion into bulk Mg (depositing the Li from a lithium borohydride diglyme electrolyte solution). The data in Figure 7a shows a CV measured on a Mg macroelectrode (r = 2.5

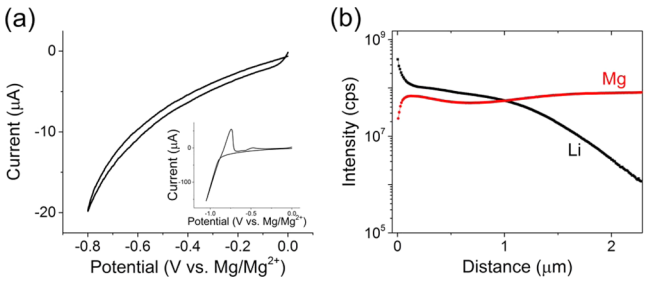

Figure 7. (a) CV obtained from a Mg macroelectrode (r = 2.5 mm) immersed in a dyglyme solution containing 1.5 M $LiBH_4$ from 0 to −0.8 V, and (inset) 0 to −1 V; (b) depth profile from a lithiated Mg at E_{Lit} = −0.8 V for 5 h in 1.5 M $LiBH_4$ diglyme solution.

mm) immersed in 1.5 M $LiBH_4$ diglyme solution. The reduction current, seen in Figure 7a, occurs from 0 to −0.8 V, which is ca. 0.1 V more positive than an onset potential of bulk Li_{Dep}, as shown in the inset of Figure 7a. A lithiating potential, E_{Lit} = −0.8 V was applied to the Mg macroelectrode for 5 h, and SIMS was performed (Figure 7b). The data strongly suggests a facile interdiffusion of the Li into the Mg base electrode is occurring under these conditions. An effective penetration length was estimated from the surface down to a point where the intensity of the Li signal dropped two orders of magnitude. From this distance, an estimate can be made of the diffusion coefficient, D_{Li} estimated to be ∼1.53 (±0.13) × 10^{-12} cm^2/s.

On the basis of these electrochemical, physical, and spectroscopic analyses, we can fully confirm the electrodeposition of a Mg−Li alloy and its dissolution in 0.1 M

DOI: 10.1021/am507375t
ACS Appl. Mater. Interfaces 2015, 7, 2494−2502

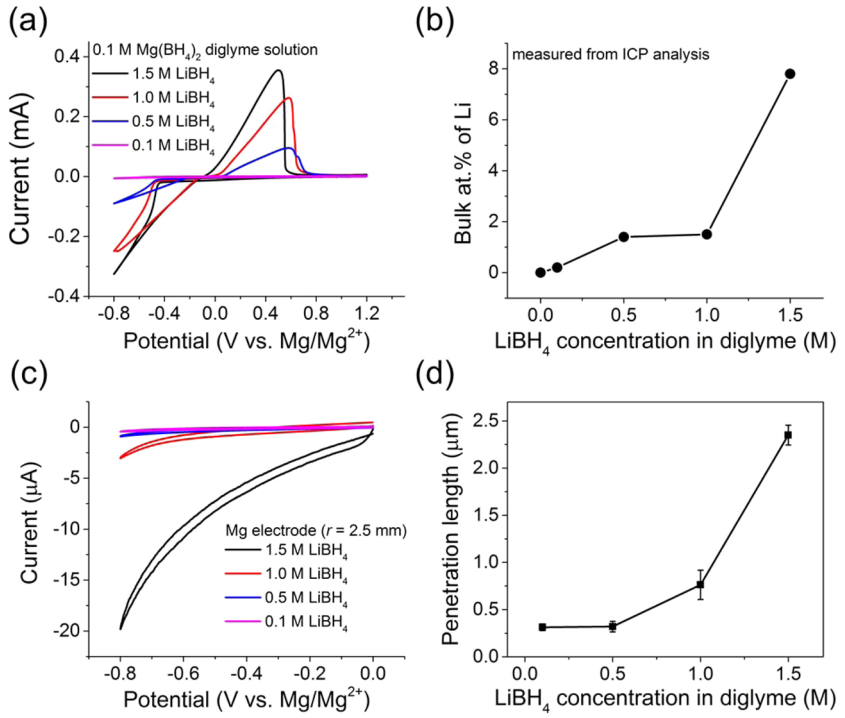

Figure 8. (a) First-cycle CVs on a Pt macroelectrode (r = 2.5 mm) in 0.1 M $Mg(BH_4)_2$ diglyme solution with 0.1, 0.5, 1.0, and 1.5 M $LiBH_4$, (b) at. % of Li in bulk Mg–Li deposits measured from ICP analysis, (c) CVs on a Mg macroelectrode (r = 2.5 mm) in diglyme solution with 0.1, 0.5, 1.0, and 1.5 M $LiBH_4$, and (d) effective penetration length estimated by depth profiling from lithiated Mg at E_{Lit} = −0.8 V for 5 h in diglyme solution with different $LiBH_4$ concentration.

$Mg(BH_4)_2$ + 1.5 M $LiBH_4$ diglyme solution. We tentatively assign the three stripping peaks observed in the CV measured at E_{Red} = −0.8 V in a 0.1 M $Mg(BH_4)_2$ + 1.5 M $LiBH_4$ diglyme solution on a Pt UME to the following formal dissolution reactions:

$$Mg_{(1-y)}Li_y \rightarrow (1-y)Mg^{2+} + yLi^{+} + (2-y)e^{-},\quad 0.02 < y \leq 0.09 \quad \text{(peak A)} \tag{3}$$

$$Mg_{(1-x)}Li_x \rightarrow (1-x)Mg^{2+} + xLi^{+} + (2-x)e^{-},\quad 0 < x \leq 0.02 \quad \text{(peak B)} \tag{4}$$

$$Mg \rightarrow Mg^{2+} + 2e^{-} \quad \text{(peak C)} \tag{5}$$

The less noble Li–Mg alloy phases are stripped first, followed by low [Li]/bulk Mg, the loss of which is detected in peak C.

The stripping voltammetry described in this report follows mechanistic trends described in the earlier studies of the electrodeposition of various binary alloys. De Long et al.[24] reported on the electrodeposition of a Co–Al alloy from room temperature chloroaluminate molten salts, and observed a CV with three distinct stripping peaks attributed to the dissolution of Co and Co–Al alloys with different Al compositions. Hussey et al.[32] reported on electrodeposited Ni–Al alloys, and observed two stripping peaks associated with the dissolution of Ni and a Ni–Al alloy. These precedents strongly support the assignments made here for the Mg/Li system.

3.3. Characterization of Mg–Li Alloy Formation: Dependence on $LiBH_4$ Concentration in a Diglyme Electrolyte Solution. Figure 8a shows first-cycle CVs measured on a Pt macroelectrode immersed in 0.1 M $Mg(BH_4)_2$ diglyme solutions with different $LiBH_4$ concentrations. The presence of different amounts of Li in solution perturbs the current densities associated with both the deposition and stripping steps, trends similar to those previously reported.[5] The differences in current density, we note, could be associated with either the presence of more Li in the Mg–Li alloy or changes in solution characteristics important to the electrochemistry (or both in some measure). The data presented below provide useful insights here.

We first examined the importance of a reduction in uncompensated resistance, R_u, which occurs with increasing $LiBH_4$ concentration. The $LiBH_4$ acts as a supporting electrolyte serving to increase conductivity of the borohydride diglyme electrolyte and reduce ohmic polarization.[33] The magnitude of R_u was measured in 0.1 M $Mg(BH_4)_2$ diglyme solutions with different $LiBH_4$ concentrations (data shown in Figure S7, Supporting Information).[20] As the $LiBH_4$ concentration was increased from 0.1 to 0.5 M, R_u decreased from 8.0 to 2.0 kΩ before attaining a limiting value of 0.8 kΩ at 1.5 M $LiBH_4$. Therefore, the $Mg_{Dep/Dis}$ kinetics is enhanced as the $LiBH_4$ concentration in the diglyme electrolyte solution increases from 0.1 to 0.5 M mainly because of the greatly reduced R_u in the solution.

The very large changes in the $Mg_{Dep/Dis}$ kinetics, data for which are shown in Figure 8a (measured at 1.0, 1.5 M $LiBH_4$ concentration), cannot be associated with a reduction R_u alone as the values of its estimated maximum iR drop in 1.0 and 1.5 M $LiBH_4$ diglyme solution are 0.263 and 0.260 V, respectively. This 3 mV difference cannot explain the significant current density increase seen in Figure 8a.

Because the electrodeposition process involves Mg–Li alloying and dissolution, the kinetics of this process must also be affected by the amount of Li available for Mg–Li alloy

DOI: 10.1021/am507375t
ACS Appl. Mater. Interfaces 2015, 7, 2494–2502

formation and the nucleation/steady-state growth mechanism that sustains it. This impact is clearly revealed in the data presented in Figure 8b, which shows the at.% of Li in the bulk Mg−Li deposit significantly increases from 1.4 to 7.8% as $LiBH_4$ concentration in diglyme solution was increased from 1.0 to 1.5 M. The increased current densities observed in solutions with higher Li concentrations must therefore be associated with the formation of alloys that are more Li-rich, an influence implicitly suggesting a facilitation of the underlying atomistic mechanisms in some form.

The data presented in Figure 8c, which investigates the lithiation kinetics on Mg with different $LiBH_4$ concentrations, sheds some insight on the latter point. From the CVs shown in Figure 8c, the lithiation kinetics evidenced at a Mg macroelectrode are in fact greatly enhanced as the $LiBH_4$ concentration in the diglyme solution are increased. As one might expect, the data presented in Figure 8d further shows that the effective penetration length of Li into the Mg increases as well with this increase in the solution Li concentration. In other words, the phase dynamics for electrochemical growth are both facilitated for the binary compositions (relative to either metal alone) and, to a strong degree, rate dependent. A stable, nondepleting Li^+ flux is needed to sustain a form of growth that, in its absence, occurs with a rather high overpotential (a correlated argument exists for Li growth in the presence of Mg^{2+}). In their combination, direct deposition of the binary phase is both preferred and subject to direct mediation via transport constraints. The important question that arises here is one related to the atomistic attributes of the electrodeposition dynamics. We believe that the codeposition behaviors of Li on Mg provide some insight into the latter. The, data especially that of Figure 7, show a strong facilitation of heteroatomic deposition in the binary composition electrolytes. For example, Li is very efficiently deposited on Mg in small quantities near 0 V versus Mg/Mg^{2+}. The corollary is that Mg^{2+}, as it exists in this electrolyte, does not. The Li so deposited then changes this attribute in a very marked way. This, we believe, provides an opportunity for both theory and advanced atomic-resolution in situ characterization tools to fully affirm and specify the nature of the bimetallic interactions that both mediate and accelerate the electrochemical deposition and stripping of divalent Mg.

4. CONCLUSIONS

In the discussions presented above, we have established the features of a synergistic mechanism for the reversible electrochemical deposition/stripping of Mg, one exhibiting an enhanced efficiency for this divalent electrochemical system. The data establish that the presence of Li cations in a $Mg(BH_4)_2/LiBH_4$ diglyme electrolyte solution leads to the codeposition of $Mg_{(1-x)}Li_x$ alloys. These alloys are Mg-rich compositions that incorporate Li in concentrations reaching as high as 9 atomic percent. Most significantly, the thermodynamic efficiencies of the metal deposition processes are greatly enhanced, as evidenced by a rather large reduction in the overpotential. The compositions of the alloys scale very sensitively with both the deposition potential and solution-based mass-transfer effects. The influences noted in the deposition process are also accompanied by striking rate/structure/composition correlations evidenced in the potential-dependent dynamics of metal stripping processes.

Taken together, the data suggest an intriguing possibility that electrolyte systems optimized for alloy (or intermetallic, or both) compositions might be developed to explicitly enhance the reversible electrochemical efficiencies of metal electrode systems of interest for use in advanced, high-energy-density electrochemical energy storage systems.

■ ASSOCIATED CONTENT

Supporting Information

Estimation of diffusion coefficient of Mg^{2+}−diglyme−BH_4^- complex by chronoamperometry; CV on a Pt UME in a diglyme electrolyte solution containing 0.01 M $Mg(BH_4)_2$ without $LiBH_4$; CV on a Pt UME in a diglyme electrolyte solution containing 0.1 M $Mg(BH_4)_2$ with 1.5 M $NaBH_4$; SIMS depth profile of a bare $Pt/SiO_2/Si$ substrate; wide-range XPS spectrum from a Mg−Li film electrodeposited at E_{Red} = −0.8 V for 5 h in a diglyme electrolyte solution containing 0.1 M $Mg(BH_4)_2$ with 1.5 M $LiBH_4$; measured R_u in a diglyme electrolyte solution containing 0.1 M $Mg(BH_4)_2$ with different $LiBH_4$ concentration; and SEM image of a Mg−Li film electrodeposited at E_{Red} = −0.8 V for 1 h in a diglyme electrolyte solution containing 0.1 M $Mg(BH_4)_2$ + 1.5 M $LiBH_4$. This material is available free of charge via the Internet at http://pubs.acs.org.

■ AUTHOR INFORMATION

Corresponding Authors

*E-mail: agewirth@illinois.edu.
*E-mail: r-nuzzo@illinois.edu.

Funding

Funding for this work was provided by the Joint Center for Energy Storage Research (JCESR), an Energy Innovation Hub funded by the U.S. Department of Energy (DE-AC02−06CH11357).

Notes

The authors declare no competing financial interest.

■ ACKNOWLEDGMENTS

J.C. thanks to Dr. Mauro Roberto Sardela for his helpful discussion about XRD measurement and results, Dr. Rudiger Laufhutte for ICP measurements, Dr. Honghui Zhou for her help with SEM measurements, and David Wetzel for his help to set up all glovebox experiments. XPS, SIMS, and XRD measurements were carried out in the Frederick Seitz Materials Research Laboratory Central Research Facilities, University of Illinois.

■ REFERENCES

(1) Yoo, H. D.; Shterenberg, I.; Gofer, Y.; Gershinsky, G.; Pour, N.; Aurbach, D. Mg Rechargeable Batteries: An On-Going Challenge. *Energy Environ. Sci.* **2013**, *6*, 2265−2279.

(2) Aurbach, D.; Lu, Z.; Schechter, A.; Gofer, Y.; Gizbar, H.; Turgeman, R.; Cohen, Y.; Moshkovich, M.; Levi, E. Prototype Systems for Rechargeable Magnesium Batteries. *Nature* **2000**, *407*, 724−727.

(3) Muldoon, J.; Bucur, C. B.; Oliver, A. G.; Zajicek, J.; Allred, G. D.; Boggess, W. C. Corrosion of Magnesium Electrolytes: Chlorides—The Culprit. *Energy Environ. Sci.* **2013**, *6*, 482−487.

(4) Muldoon, J.; Bucur, C. B.; Oliver, A. G.; Sugimoto, T.; Matsui, M.; Kim, H. S.; Allred, G. D.; Zajicek, J.; Kotani, Y. Electrolyte Roadblocks to a Magnesium Rechargeable Battery. *Energy Environ. Sci.* **2012**, *5*, 5941−5950.

(5) Mohtadi, R.; Matsui, M.; Arthur, T. S.; Hwang, S. J. Magnesium Borohydride: From Hydrogen Storage to Magnesium Battery. *Angew. Chem., Int. Ed. Engl.* **2012**, *51*, 9780−9783.

(6) Shao, Y.; Liu, T.; Li, G.; Gu, M.; Nie, Z.; Engelhard, M.; Xiao, J.; Lv, D.; Wang, C.; Zhang, J. G.; Liu, J. Coordination Chemistry in

DOI: 10.1021/am507375t
ACS Appl. Mater. Interfaces 2015, 7, 2494−2502

Magnesium Battery Electrolytes: How Ligands Affect Their Performance. *Sci. Rep.* **2013**, *3*, 3130.
(7) Heinze, J. Ultramicroelectrodes in Electrochemistry. *Angew. Chem., Int. Ed. Engl.* **1993**, *32*, 1268−1288.
(8) Malmsten, R. A.; White, H. S. Voltammetric Studies Beyond the Solvent Limits with Microelectrodes. *J. Electrochem. Soc.* **1986**, *133*, 1067−1068.
(9) Malmsten, R. A.; Smith, C. P.; White, H. S. Electrochemistry of Concentrated Organic Redox Solutions. *J. Electroanal. Chem.* **1986**, *215*, 223−235.
(10) Morris, R. B.; Fischer, K. F.; White, H. S. Electrochemistry of Organic Redox Liquids—Reduction of 4-Cyanopyridine. *J. Phys. Chem.* **1988**, *92*, 5306−5313.
(11) Bond, A. M.; Mann, T. F. Voltammetric Measurements without Ohmic and Other Forms of Distortion in Aromatic Hydrocarbon Solvents. *Electrochim. Acta* **1987**, *32*, 863−870.
(12) Zhao, H.; Chang, J.; Boika, A.; Bard, A. J. Electrochemistry of High Concentration Copper Chloride Complexes. *Anal. Chem.* **2013**, *85*, 7696−7703.
(13) Yan, Y.; Zhang, M.; Han, W.; Xue, Y.; Cao, D.; Yuan, Y. Electrochemical Codeposition of Mg−Li Alloys from a Molten KCl−LiCl−$MgCl_2$ System. *Chem. Lett.* **2008**, *37*, 212−213.
(14) Yan, Y. D.; Xue, Y.; Zhang, M. L.; Han, W.; Zhang, M.; Tang, H.; Li, X.; Zhang, Z. J. Direct Electrodeposition of Quarternary Mg−Li−Al−Zn Alloys from Their Chloride Melts. *J. Electrochem. Soc.* **2011**, *158*, D317−D322.
(15) Yan, Y. D.; Zhang, M. L.; Han, W.; Cao, D. X.; Yuan, Y.; Xue, Y.; Chen, Z. Electrochemical Formation of Mg−Li Alloys at Solid Magnesium Electrode from LiCl−KCl Melts. *Electrochim. Acta* **2008**, *53*, 3323−3328.
(16) Yan, Y. D.; Zhang, M. L.; Xue, Y.; Han, W.; Cao, D. X.; Jing, X. Y.; He, L. Y.; Yuan, Y. Electrochemical Formation of Mg−Li−Ca Alloys by Codeposition of Mg, Li, and Ca from LiCl−KCl−$MgCl_2$−$CaCl_2$ Melts. *Phys. Chem. Chem. Phys.* **2009**, *11*, 6148−6155.
(17) Park, C. M.; Kim, J. H.; Kim, H.; Sohn, H. J. Li-Alloy Based Anode Materials for Li Secondary Batteries. *Chem. Soc. Rev.* **2010**, *39*, 3115−3141.
(18) Park, C.-M.; Kim, Y.-U.; Kim, H.; Sohn, H.-J. Enhancement of the Rate Capability and Cyclability of an Mg−C Composite Electrode for Li Secondary Batteries. *J. Power Sources* **2006**, *158*, 1451−1455.
(19) Huggins, R. A. Lithium Alloy Negative Electrodes. *J. Power Sources* **1999**, *81*, 13−19.
(20) Bard, A. J.; Faulkner, L. R. *Electrochemical Methods: Fundamentals and Applications*. Wiley: New York, 2000.
(21) Paddon, C. A.; Compton, R. G. Underpotential Deposition of Lithium on Platinum Single Crystal Electrodes in Tetrahydrofuran. *J. Phys. Chem. C* **2007**, *111*, 9016−9018.
(22) Paddon, C. A.; Jones, S. E. W.; Bhatti, F. L.; Donohoe, T. J.; Compton, R. G. Kinetics and Thermodynamics of the Li/Li^+ Couple in Tetrahydrofuran at Low Temperatures (195−295 K). *J. Phys. Org. Chem.* **2007**, *20*, 677−684.
(23) Moffat, T. P. Electrodeposition of $Ni_{1-x}Al_x$ in a Chloroaluminate Melt. *J. Electrochem. Soc.* **1994**, *141*, 3059−3070.
(24) Carlin, R. T.; Trulove, P. C.; De Long, H. C. Electrodeposition of Cobalt-Aluminum Alloys from Room Temperature Chloroaluminate Molten Salt. *J. Electrochem. Soc.* **1996**, *143*, 2747−2758.
(25) Carlin, R. T.; De Long, H. C.; Fuller, J.; Trulove, P. C. Microelectrode Evaluation of Transition Metal-Aluminum Alloy Electrodepositions in Chloroaluminate Ionic Liquids. *J. Electrochem. Soc.* **1998**, *145*, 1598−1607.
(26) Pelton, A. D. The Mg−Na (Magnesium−Sodium) System. *Bull. Alloy Phase Diagrams* **1984**, *5*, 454−456.
(27) Yin, L.; Cheng, H. Y.; Mao, S. M.; Haasch, R.; Liu, Y. H.; Xie, X.; Hwang, S. W.; Jain, H.; Kang, S. K.; Su, Y. W.; Li, R.; Huang, Y. G.; Rogers, J. A. Dissolvable Metals for Transient Electronics. *Adv. Funct. Mater.* **2014**, *24*, 645−658.
(28) Kurth, M.; Graat, P. C. J.; Mittemeijer, E. J. Determination of the Intrinsic Bulk and Surface Plasmon Intensity of XPS Spectra of Magnesium. *Appl. Surf. Sci.* **2003**, *220*, 60−78.
(29) Suo, L.; Hu, Y. S.; Li, H.; Armand, M.; Chen, L. A New Class of Solvent-in-Salt Electrolyte for High-Energy Rechargeable Metallic Lithium Batteries. *Nat. Commun.* **2013**, *4*, 1481.
(30) Kúdela, S.; Oswald, S.; Kúdela, S., Jr.; Baunack, S.; Wetzig, K. XPS and SIMS Examination of Alumina Fibres Affected with Mg and MgLi Melt. *Microchim. Acta* **2000**, *133*, 29−34.
(31) Awaludin, Z.; Okajima, T.; Ohsaka, T. Formation of Pt−Li Alloy and its Activity Towards Formic Acid Oxidation. *Electrochem. Commun.* **2013**, *31*, 100−103.
(32) Pitner, W. R.; Hussey, C. L.; Stafford, G. R. Electrodeposition of Nickel−Aluminum Alloys from the Aluminum Chloride-1-methyl-3-ethylimidazolium Chloride Room Temperature Molten Salt. *J. Electrochem. Soc.* **1996**, *143*, 130−138.
(33) Daniele, S.; Baldo, M. A.; Corbetta, M.; Mazzocchin, G. A. Linear Sweep and Cyclic Voltammetry for Metal-Deposition at Solid and Mercury Microelectrodes from Solutions with and without Supporting Electrolyte. *J. Electroanal. Chem.* **1994**, *379*, 261−270.

DOI: 10.1021/am507375t
ACS Appl. Mater. Interfaces 2015, 7, 2494−2502